ELSEVIER

Nuclear Physics A 634 (1998) 115-140

NUCLEAR PHYSICS A

Subthreshold antiproton production in pA, dA and αA reactions

Y. Sugaya [a,1], D. Ashery [b,2], J. Chiba [b], H. Ito [c,3], K. Kimura [d], Yu.T. Kiselev [e], S. Kouda [f,4], K. Miyano [g], T. Murakami [c], J. Murata [c], T. Nagae [b], Y. Nakai [h], M. Nomachi [b,1], M. Numajiri [b], H. Ochiishi [f], S. Sawada [c,5], M. Sekimoto [b], T. Shibata [b], T. Suzuki [h], K.H. Tanaka [b], M.K. Vlasov [e], Y. Yamanoi [b], K. Yasuda [c,1], Y. Yoshimura [b,6]

[a] *Tokyo University of Agriculture and Technology, Tokyo 184, Japan*
[b] *High Energy Accelerator Research Organization (KEK), Tsukuba 305, Japan*
[c] *Department of Physics, Kyoto University, Kyoto 606-01, Japan*
[d] *Nagasaki Institute of Applied Science, Nagasaki 851-01, Japan*
[e] *Institute of Theoretical and Experimental Physics, Moscow RU-117259, Russia*
[f] *Department of Physics, Kyushu University, Fukuoka 812-81, Japan*
[g] *Department of Physics, Niigata University, Niigata 950-21, Japan*
[h] *RIKEN, Institute of Physical and Chemical Research, Wako 351-01, Japan*

Received 3 July 1997; revised 24 December 1997; accepted 9 January 1998

Abstract

An enormous enhancement of antiproton production in deuteron- and α-induced reactions has been observed in the subthreshold energy region between 2 and 5 GeV/nucleon. Antiprotons produced at 5.1° with a momentum range of between 1.0 and 2.5 GeV/c were measured by a beam-line spectrometer and identified by the time-of-flight method. The production cross sections in the deuteron- and α-induced reactions at an incident energy of 3.5 GeV/nucleon were 2 and 3 orders of magnitude larger than those in proton-induced reaction at the same energy. The enhancement in light-ion reactions could not be explained by the internal motion in the projectile and target nuclei. The target-mass dependence (C, Al, Cu and Pb) of the cross sections has also been studied. Further, the cross sections of π and K productions were measured. © 1998 Elsevier Science B.V.

PACS: 25.45.-z, 25.55.-e, 25.75.Dw
Keywords: Antiproton production; Subthreshold; Light-ion induced reaction; Kaon production; Pion production

PII S0375-9474(98)00122-5

1. Introduction

Subthreshold antiproton production with light-ion beams is described based on experimental data and is discussed in this paper. Preliminary reports on its measurement have already been made elsewhere [1,2]. Subthreshold particle production, which is defined as production below the energy threshold in a free nucleon–nucleon collision, requires energy concentration inside of a tiny region in a nucleus. In particular, a huge concentration is necessary for antiproton production, because an antiproton is produced only in baryon-antibaryon pair production. Such an energy concentration might be caused by coherent or collective processes. However, we do not yet know the detailed mechanism; therefore, subthreshold antiproton production should be studied in many kinds of nuclear reactions. It should also be sensitive to the baryon free-energy and should help us to derive information about the thermal processes in a nucleus.

Subthreshold antiproton production was observed at the time that antiprotons were discovered by Chamberlain et al. in 1955 [3]. They observed antiprotons of 1.19 GeV/c in p+Cu reactions at incident energies of 4.2, 5.1 and 6.2 GeV and production angles of 3°, 6° and 8°, respectively. Dorfan et al. measured the antiproton-to-pion ratios from p+Cu reactions at the BEVATRON and the Princeton-Penn accelerator in 1965 [4]. They observed antiprotons having momenta from 0.76 to 1.37 GeV/c in an incident-energy range from 2.88 to 6.1 GeV. In 1987 at the synchrophasotron of the Institute of Theoretical and Experimental Physics (ITEP), Lepikhin et al. measured the antiproton production cross sections with Be, Al and Cu targets [5]. They measured 1.76 GeV/c antiprotons emitted at 188 m rad in the incident-energy range between 3.7 and 9.2 GeV. Through these studies of subthreshold antiproton production, it was concluded that production in a proton-induced reaction was caused by internal motions in the target nucleus.

Concerning nucleus–nucleus reactions, an experiment was carried out at the Joint Institute for Nuclear Research (JINR) in 1988 [6]. Baldin et al. measured the antiproton production cross sections in p+C, d+C, C+C and C+Cu reactions at an incident energy of 3.65 GeV/nucleon. Antiprotons with momenta of 0.6, 0.8 and 0.9 GeV/c were collected at 24°.

A large cross section of subthreshold antiproton production in heavy-ion reactions was found at the LBL-BEVALAC in 1989. The cross section from the Si+Si reaction was measured at an incident energy of 2.0 GeV/nucleon [7,8]. The cross section of 1.9-GeV/c antiproton production at 0° was 3 orders of magnitude larger than the cross section calculated by a model based on a nucleon–nucleon collision taking account of

[1] Present address: Research Center for Nuclear Physics (RCNP), Osaka University.
[2] On leave from Tel Aviv University 69978, Israel.
[3] Present address: Nippon Telegraph and Telephone Corporation (NTT).
[4] Present address: National Institute of Radiological Sciences.
[5] Present address: High Energy Accelerator Research Organization.
[6] Corresponding author. High Energy Accelerator Research Organization, 1-1 Oho, Tsukuba, Ibaraki, 305 Japan, tel. +81-298-64-5414, fax +81-64-7831, e-mail yoshimur@kekvax.kek.jp.

the internal motions in the target and projectile nuclei. In 1991 at GSI, Schröter et al. measured the cross section of antiproton production in heavy-ion collisions using Ne (1.6, 1.8 and 2.0 GeV/nucleon) and Ni (1.835 and 1.928 GeV/nucleon) beams [9]. They observed 1.0~2.2 GeV/c antiprotons at 0 °. This measurement confirmed the large cross section in heavy-ion reactions at BEVALAC.

Theoretical calculations have been performed in an attempt to understand the mechanisms of antiproton production in heavy-ion reactions. Ko et al. tried thermal models, which resulted in a sizable antiproton-production cross section for the experiment at BEVALAC [10,11]. They examined antiproton production mechanisms through the $\pi\pi$, $\eta\eta$, $\rho\rho$ and $\omega\omega$ collisions, finding that the ρ mesons produced in a fireball play an important role for antiproton production in the energy region of BEVALAC. Koch et al. also claimed that the ΔN and $\Delta\Delta$ collisions can result in large antiproton-production cross sections [12]. However, the point is whether or not the Δ and ρ production cross sections are large enough. Batko et al. made a calculation based on the Vlasov–Uehling–Uhlenbeck transport theory (VUU) [13]. This calculation could reproduce the BEVALAC data by including multiple scattering and the intermediate states of Δ and N^*. Huang et al. also obtained large antiproton-production cross sections by relativistic quantum molecular dynamics (RQMD) [14]. However, these calculations had large ambiguities concerning the reabsorption and production cross-section in elementary processes. Although an antiproton can be reabsorbed with a large probability by the nucleus which produced it, the process is difficult to consider. Antiproton-production cross sections have so far not been measured in the elementary process at energies below 13 GeV [13,15]. In these calculations, the cross sections near to the threshold (5.63 GeV) are obtained in terms of an extrapolation of data at higher energies.

Our experiment was motivated by the large cross sections for subthreshold antiproton production in heavy-ion reactions. Subthreshold antiproton-production with light-ion beams, such as deuterons or α particles, is useful to ensure the theoretical models, because the chance of multiple scattering is smaller than that in a heavy-ion reaction. Light-ion induced reactions do not produce hot, dense nuclear matter, which is employed by the thermal model, because of the small total energy of the projectile. It is a good test of these models to see if they can reproduce light-ion induced reactions.

In Section 2 the experimental apparatus and methods are described. The analysis used to deduce the production cross-sections is discussed in Section 3. The cross sections of subthreshold antiproton production are described in Section 4. Pion- and kaon-production cross sections in this experiment are also shown, partly as a check of the experimental method. In Section 5 the cross sections are calculated employing a model which takes into account the internal motions of nucleons within nuclei. A summary of this paper is given in Section 6.

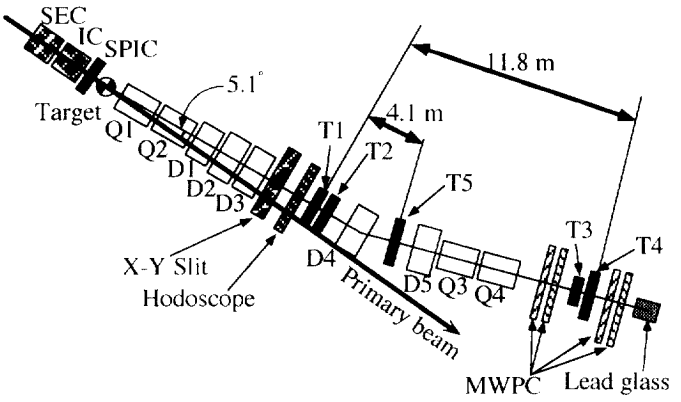

Fig. 1. Schematic view of the experimental setup. The T3 beam-line spectrometer consists of five dipole (D1~5) and four quadrupole magnets (Q1~4) and an X-Y slit. T1~T5 are scintillation counters for TOF measurements.

2. Experiment

A series of experiments was carried out at the proton synchrotron in the High Energy Accelerator Research Organization (KEK-PS) where deuteron beams have been available since 1992 and α beams since 1994. These experiments were the first ones with light-ion beams at the KEK-PS. Great care was taken concerning the intensity and profile measurements of these primary beams. Fig. 1 shows a schematic view of the experimental setup. This experiment was carried out at the EP2 primary beam-line and T3 secondary beam-line. The produced particles were analyzed using the T3 beam-line as a momentum spectrometer, and were identified by a time-of-flight (TOF) measurement.

The typical beam intensities in the main ring were 4×10^{12}, 2×10^{12} and 5×10^{10} particle per pulse for proton, deuteron and α beams, respectively. About half of them were delivered on a target. The intensity of the primary beams was measured by a secondary emission chamber (SEC) [16], which was calibrated using 12-GeV proton beams by radiochemical methods [17]. Calibration runs were made both before and after the experiment, and the response of the SEC did not change. The SEC response for different particles (deuteron and α) at different energies was calibrated by comparing the measurements with an ionization chamber (IC), radiochemical methods and pion-production cross-sections [18]. The measurement of the primary beam profile was important, because the acceptance of the spectrometer depended on the beam position on the target. We thereby measured the beam profile every eight hours using a segmented parallel-plate ionization chamber (SPIC) just upstream of the production-target position [19].

The targets were blocks of carbon, aluminum and copper. The thicknesses, chosen to be less than 10% of the interaction length, were 6.9, 10.8 and 13.4 g/cm^2 respectively. A lead target with a thickness of 17.0 g/cm^2 was used for both the deuteron beams and a 12-GeV proton beam in order to study the reabsorption of antiprotons in the target nucleus.

Particles which were emitted at an angle of 5.1° entered the spectrometer. The momentum of the outgoing particles was selected by five dipole and four quadrupole magnets and an X–Y slit. The slit width was adjusted while taking into consideration the trigger rate and the counting rate of the detectors. In consequence the antiproton acceptances were typically 0.45 m sr % for proton and deuteron beams and 1.3 m sr % for α beams.

Two-stage TOF measurements were performed with three sets of plastic scintillation counters. Start counters (T1, T2) were placed 18.7 m from the target on the axis of the outgoing particles. The distance between the start and stop counters (T3, T4) was 11.8 m. The start counters consisted of two $60 \times 100 \times 5$ mm^3 plastic scintillators at an interval of 75 mm. The stop counters (T3 and T4) were also plastic scintillators located 50 mm apart. In order to check the beam focus and background, different sizes of $50 \times 50 \times 10$ mm^3 (T3) and $100 \times 100 \times 10$ mm^3 (T4) were chosen. An additional intermediate counter (T5; $90 \times 150 \times 5$ mm^3) was placed 4.1 m behind the start counters. This was used to distinguish background events in an off-line analysis. Two photomultipliers (H2431) were mounted on both sides of each scintillator (Pilot U). The setup mentioned above was for an experiment with α beams. The distances between the counters were slightly different for the experiment with the other beams. The profiles of outgoing particles were measured using a hodoscope upstream of T1 and MWPCs both upstream and downstream of the stop counters in order to ensure a focus of the outgoing particles and to facilitate acceptance calculations. The hodoscope measured the profiles horizontally with a 4.4 mm step, and the MWPCs horizontally and vertically with a 2 mm step. A lead-glass Cherenkov counter was put on the tail of the setup to separate electrons from pions.

The event trigger was produced by the coincidences of signals from the start and stop TOF counters. The event trigger provided gates for digitizing the detector signals as well as an interrupt signal for data read-out. Antiprotons and pions could not be collected by the same trigger setup because of an enormous cross-section difference of the particle production ($\pi/\overline{p} \sim 10^5$). The pulses from the start and stop counters were adjusted so as to make a coincidence for the antiproton event in order to reject pions ($\overline{p}$-trigger). Since the TOF of a pion between the start and stop counters was sufficiently smaller than that of an antiproton, the pion events could be rejected at the trigger level by setting the coincidence window. Other coincidence with a wider pulse from the stop counter, which was prescaled down by three orders, was also prepared to measure the cross sections of pion production (π-trigger). The cross sections of positive pions and kaons were also measured by changing the polarity of beam-line magnets and using an unprescaled π-trigger.

3. Data analysis

The differential cross section of particle production is expressed by the following formula:

Table 1
Systematic error on a cross section

	Relative error
Beam intensity measurement	12%
Acceptance calculation	10%
Correction for loss due to interaction	5%
Correction for loss due to analytical cuts	1%
Correction for decay	1%

$$\frac{d^2\sigma}{dp\,d\Omega} = \frac{N_p/C_{corr}}{N_b \times N_t \times (\Delta\Omega\Delta p/p) \times p}. \tag{1}$$

Here, N_p is the number of particles detected. N_b is the number of projectile particles, N_t the number of target nuclei per unit area, $\Delta\Omega\Delta p/p$ the geometrical acceptance of the spectrometer, p the momentum of the outgoing particle and C_{corr} a correction factor, which can be written as

$$C_{corr} = C_c \times C_m \times C_d \times C_t. \tag{2}$$

Here, C_c is a correction factor for the loss of events due to various cuts for a yield evaluation, C_m for the particle loss due to interactions with materials in the spectrometer, C_d for the decay of particles and C_t for the dead-time of data acquisition. The systematic errors on the obtained cross section (discussed in following section) are summarized in Table 1.

3.1. Primary-beam intensity

For experiments using secondary beams, such as kaons or pions at KEK-PS, the intensity of 12-GeV proton beams is normally monitored by a secondary emission chamber (SEC). The calibration factor of the SEC for 12-GeV proton beams has been obtained by radiochemical methods using thin aluminum foils. After studying the response for different energies and different beam particles, the SEC was also used as the main detector for primary-beam intensity measurements in this experiment. Since secondary electron emission is one of the processes governed by electromagnetic interactions, the charge yields from the SEC might be proportional to the square of the particle's Z-number, and do not strongly depend on the particle's energy in the GeV region. Therefore, once the SEC is calibrated with 12-GeV proton beams, it can be used to measure the intensity of other particles at a different energy. In order to verify this assumption, the calibrations of the SEC were carried out by radiochemical methods with reactions of ^{27}Al(p,spallation)^{7}Be, ^{27}Al(p,3pn)^{24}Na, ^{27}Al(d,3p2n)^{24}Na, ^{12}C(α,αn)^{11}C, ^{12}C(α,spallation)^{7}Be and ^{27}Al(α,spallation)^{24}Na [17]. Thin films were exposed to a beam, and the numbers of ^{7}Be, ^{11}C and ^{24}Na were obtained by counting gamma rays from their decay. An additional check of SEC was performed with an ionization chamber (IC), which was calibrated with 12-GeV proton beams. Since the

Table 2
Result of the beam-intensity calibration

Beam	Energy (GeV/nucleon)	$N_{acti}(^{11}C)/N_{SEC}$	$N_{acti}(^{7}Be)/N_{SEC}$	$N_{acti}(^{24}Na)/N_{SEC}$	N_{IC}/N_{SEC}
p	5.0	–	1.23	1.03	–
p	4.0	–	1.12	0.98	–
d	5.0	–	–	0.68	1.02
d	4.0	–	–	0.74	1.05
d	3.0	–	–	0.68	1.02
α	5.0	0.93	1.13	0.85	0.97
α	3.0	0.98	1.04	0.87	0.99
α	2.0	0.96	1.03	–	0.96

energy loss of a charged particle in gas obeys the Bethe–Bloch equation, the response of the IC can be exactly estimated for the beam intensity of other particles with different energies.

The ratio of the measured intensities (N_{acti}/N_{SEC}, N_{IC}/N_{SEC}; here, N_{SEC} denotes the beam intensity measured by the SEC, N_{acti} by radiochemical methods, and N_{IC} by the IC) is summarized in Table 2. The radiochemical methods gave similar results within the accuracy of the methods, except for the deuteron beams, while the SEC measurement agreed well with the IC in all cases. The SEC response was also confirmed using the pion-production cross sections, as discussed in a later section. We therefore concluded that the disagreement in the intensity measurements for a deuteron beam is due to ambiguity in the cross section used for the radiochemical method. After these studies, the intensities of proton, deuteron and α beams were determined by the SEC. The ambiguity of the absolute intensity was estimated to be 12%, which mainly come from the error of the radiochemical method.

3.2. Beam-line simulation

The acceptance of the spectrometer ($\Delta\Omega \times \Delta p/p$) was calculated by a Monte Carlo simulation code, TURTLE. TURTLE was modified to take into account multiple Coulomb scattering, as well as absorption and energy loss by materials in the spectrometer [20]. The correction factors for particle losses due to the interaction with the materials (C_m) and for the decay of the particles (C_d) were also calculated by TURTLE.

The calculation of the spectrometer acceptance was carried out using profiles and positions of primary beams measured by the SPIC. Since the beam position didn't move significantly, the fluctuations of the acceptances were less than ±5%.

A measurement using different primary beam positions was carried out during beam-line turning. A measurement for different X–Y slit widths was also performed. The acceptance calculation was checked in terms of seeing how much it reproduce these different situations. The ratio of the particle yields for the different beam positions and

the slit widths were reproduced based on the calculated acceptance within 10% accuracy. Therefore, we take the systematic error of the acceptance calculation as being 10%.

Some of the produced particles were lost due to interactions with the materials in the spectrometer. The correction factor for this loss (C_m) was also estimated by TURTLE. The interactions taken into account in this calculation were Coulomb multiple scattering, energy loss and absorption of the produced particle by the materials, including the target, air, stainless steel and plastic scintillators. The antiproton-absorption cross section was taken from Ref. [21]. The correction factor (C_m) was obtained by making the calculation while switching off and on these interactions, and is the ratio of the fractions of particles arriving at the end of the spectrometer. C_m, which depends on the momentum of the produced particle, is 0.56 for a 1.0 GeV/c antiproton with a copper target, and 0.80 for 2.5 GeV/c. C_m also depends slightly on the kind of target and particle species. A systematic error on C_m was estimated by changing the interaction cross-section by $\pm 10\%$; C_m then changed within 3%. Consequently, the systematic error of C_m is taken to be 5%, including errors in the parameterization for these interactions.

Some of the daughter muons from the decay were identified as being parent kaons or pions based on TOF measurements. The fraction of the muon contamination on parent particles was estimated by using TURTLE. TURTLE can calculate how the daughter particle continues to fly after decay. The correction factor for decay (C_d) is determined by the survival rate, $\exp(-\ell m/cp\tau)$, and the muon contamination, where ℓ is the distance from the target to the stop counters (30.5 m), c is the light velocity, and m, p and τ are the mass, momentum and lifetime of the particle, respectively. The survival rates for pions range from 0.58 (1.0 GeV/c) to 0.80 (2.5 GeV/c) and from 0.017 to 0.20 for kaons in the measured momentum region. The contaminations of daughter muons are 5~6% for pions and 3~4% for kaons depending on the particle momentum. The contamination for kaons is smaller than that for pions, because the muon which was produced before the start counters could be discriminated from kaons by the TOF measurement. The uncertainty of C_d is at most 1%, which is mainly caused by muon contamination.

3.3. Yield evaluation

Fig. 2 shows a typical TOF distribution from T1 to T4 for 1.5 GeV/c negative charged particles taken with the $\bar{p}$-trigger. The continuous background hid the antiproton peak at a lower incident energy or higher momentum of the outgoing particle, where $\bar{p}/\pi$ is small. The background was an accidental coincidence of two independent pions. In a two-dimensional plot between the upstream TOF (from T1 to T5) and the downstream TOF (T5, T4) of Fig. 3, these accidental events are shown in the horizontal and vertical bands at the pion-timing. The background bands were made of events in which the first pion struck the start counters, but did not strike the stop counters, and a second pion struck the stop counters within several nano seconds. Since both of the pions which made this accidental coincidence hit the start counters (T1, T2), the pulse-height distribution of the start counters had an additional energy deposit due to pile-up (Fig. 4a). When

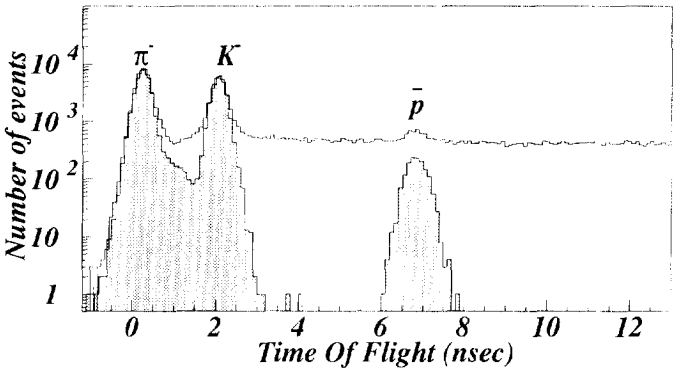

Fig. 2. Typical distribution of TOF for events of 1.5-GeV/c particles taken with the $\bar{p}$-trigger. The open histogram shows the distribution without any cuts. The hatched histogram shows the distribution after cuts. The reaction is α+C at an incident energy of 5.0 GeV/nucleon.

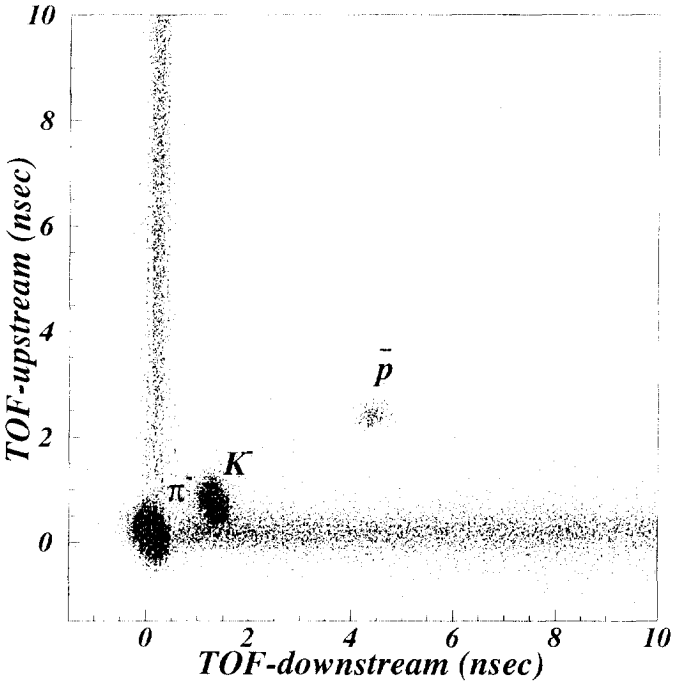

Fig. 3. Typical two-dimensional plot between upstream and downstream TOF for events of 1.5-GeV/c particles taken with the $\bar{p}$-trigger. The reaction is α+C at 5.0 GeV/nucleon.

events with small pulse heights in both start counters were selected, the background was sufficiently rejected. The antiproton yields were obtained from the distribution after a pulse-height cut (Fig. 4b). The number of events lost by the pulse-height cut was estimated using pulse-height distributions of antiprotons which were produced in a 12-GeV proton induced reaction where antiprotons can be identified without a pulse-hight cut. The factor used to correct the event loss due to the pulse-height cut was 0.95~0.97.

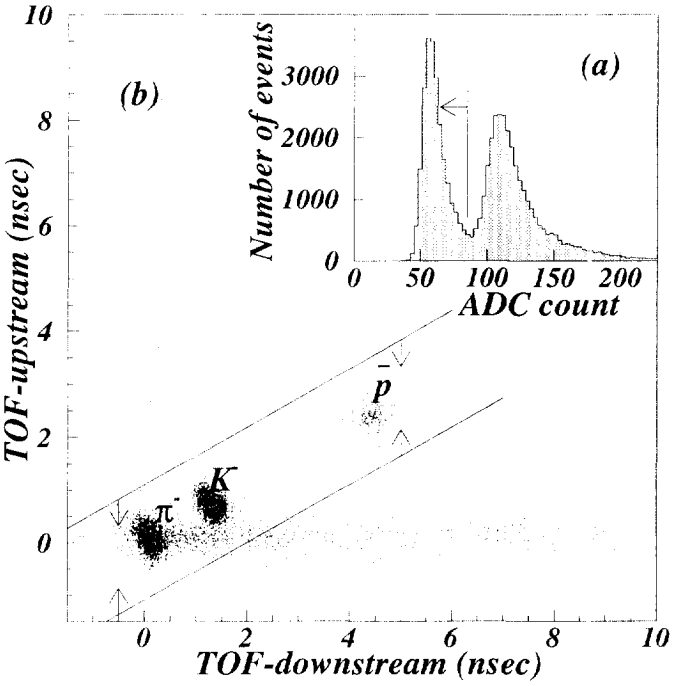

Fig. 4. (a) Pulse-height distribution of T1 and (b) two-dimensional plot between upstream and downstream TOF for events of 1.5-GeV/c particles taken with $\bar{p}$-trigger after cutting by the pulse hight. The event in the region between two lines are accepted. The reaction is α+C at 5.0 GeV/nucleon.

The yield of kaons was also obtained by employing the same method. The pion yield was obtained from events taken by the π-trigger. There was almost no background.

4. Result

Fig. 5 shows the differential cross sections of antiproton production at 1.5 GeV/c from proton-, deuteron- and α-induced reactions on a copper target as a function of the incident energy. At an incident energy of 3.5 GeV/nucleon those in deuteron- and α-induced reaction are 2 and 3 orders of magnitude larger than that from a proton-induced reaction, respectively. The lower is the incident energy, the larger is the cross section ratio between the proton-, deuteron- and α-induced reactions.

The cross sections in the heavy-ion reactions at GSI are also plotted in Fig. 5. In the Ne+Cu reaction the cross section is about 30-times larger than that in the α-induced reaction at an incident energy of 2.0 GeV/nucleon. It seems that the cross sections of antiproton production in the p+Cu reaction at the Institute of Theoretical and Experimental Physics (ITEP) [5] are consistent with our data, though they were measured at a different angle. Deuteron- and α-induced reactions produce antiprotons with higher momentum than the proton-induced reaction, as shown in Fig. 6. The increase of higher momentum antiprotons suggests that the deuteron- and α-induced

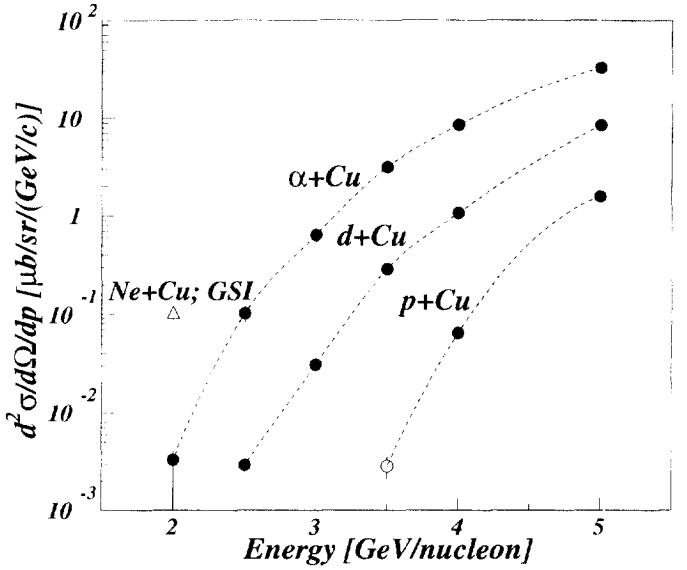

Fig. 5. Production cross sections of an antiproton with momentum of 1.5 GeV/c as a function of the incident energy per nucleon. The symbol (○) means a cross section derived from data with a carbon target assuming the target-mass dependence of $A^{2/3}$. A cross section in the Ne-induced reaction at GSI (△) [9] is also shown.

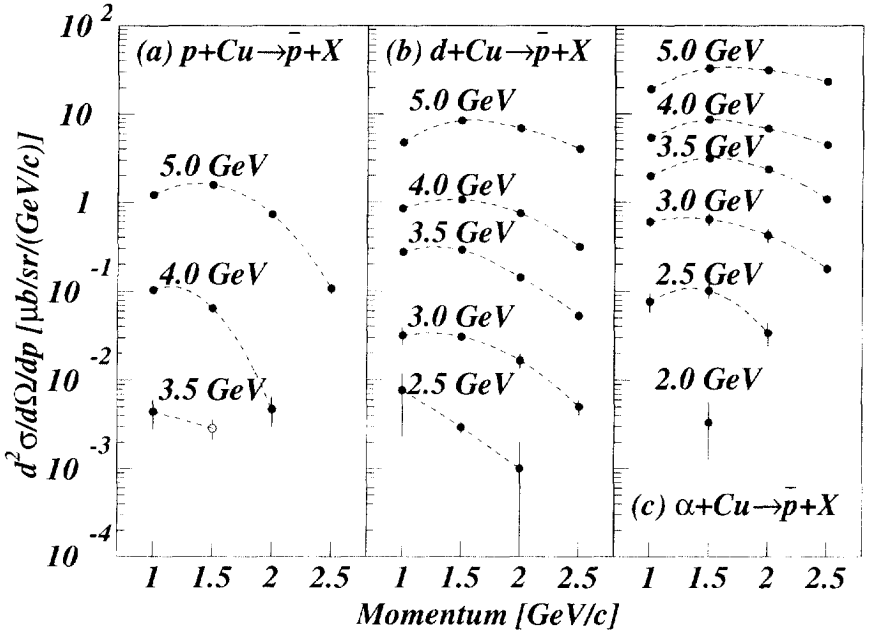

Fig. 6. Momentum spectra of antiproton production with a copper target. Data at the same energy (GeV/nucleon) are joined to guide the eyes.

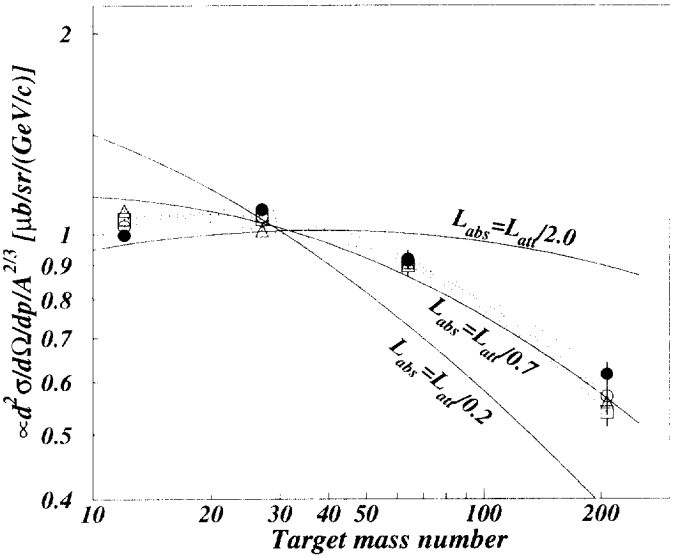

Fig. 7. Target-mass dependence of antiproton production at a deuteron incident-energy of 4.0 GeV/nucleon. The cross section is divided by $A^{2/3}$ and then normalized so that the average of data from carbon, aluminum and copper targets is unity. The momenta of antiprotons are 1.0 (•), 1.5 (○), 2.0 (△) and 2.5 (□) GeV/c. The solid lines show the calculated A-dependence with the fixed attenuation length of a projectile ($L_{\rm att}$ = 2.7 fm) and various absorption lengths of antiproton ($L_{\rm abs}$) in a nucleus. See text for details.

reactions aren't quasi-free processes anymore. It is also seen on our simulation in the following section.

The cross section depends on the target mass (A), being roughly proportional to $A^{2/3}$ in the mass region from carbon through copper. For lead, a deviation from the $A^{2/3}$-dependence is found over the deuteron-energy region which we measured. The cross sections of the deuteron-induced reaction at 4.0 GeV/nucleon are shown in Fig. 7, divided by $A^{2/3}$. They are multiplied by a normalization factor, which makes the average among carbon, aluminum and copper to be unity at each momentum. The solid line in the figure is the result of a simple model calculation considering the attenuation of the projectiles and the reabsorption of antiprotons. The attenuation length of the projectile in a nucleus is taken to be 2.7 fm, assuming that the nucleus has a spherical shape with a radius of $1.2A^{1/3}$ fm and a uniform density. The inelastic cross section in a nucleon–nucleon collision is assumed to be 27 mb. The calculation was performed by integrating the attenuation and reabsorption over the nucleus for three cases of the absorption lengths: 2.7/2, 2.7/0.7 and 2.7/0.2 fm. The reabsorption length of 2.7/0.7 fm well reproduces the A-dependence in our experiment. This value corresponds to an absorption cross section of ~20 mb in the $\overline{p}$+nucleon reaction. This is smaller than the inelastic cross section of the $\overline{p}$+nucleon reaction (~60 mb for $\overline{p}+p$) [22]. The small absorption of antiprotons, which are produced in a nucleus, is also reported in Ref. [23].

The cross sections of pion and kaon production were measured at the same time, and are given in Tables A.4–A.15. The pion-production cross sections can be used to check

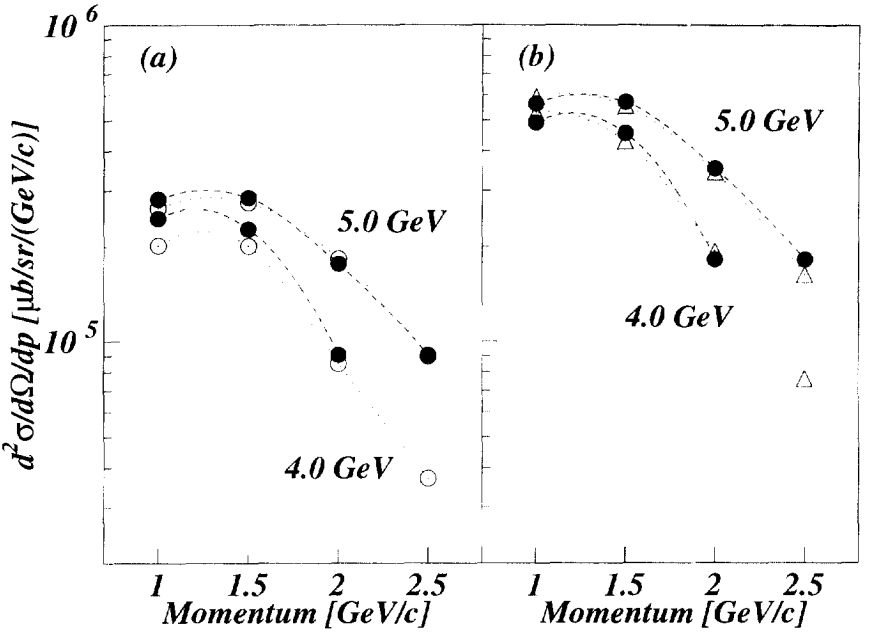

Fig. 8. Pion-production cross sections; (a) $d^2\sigma(p + C \rightarrow \pi^- + X) + d^2\sigma(p + C \rightarrow \pi^+ + X)$ (•) and $d^2\sigma(d + C \rightarrow \pi^- + X)$ (○) and (b) $2 \times \{d^2\sigma(p + C \rightarrow \pi^- + X) + d^2\sigma(p + C \rightarrow \pi^+ + X)\}$ (•) and $d^2\sigma(\alpha + C \rightarrow \pi^- + X)$ (△). The statistical error bar is smaller than the symbols.

the experimental procedures, including a beam-intensity calibration. It can be supposed that pions are produced in a quasi-free process at high energies. The relation between these cross sections in proton- and deuteron-induced reactions is thus written as

$$\begin{aligned}\sigma(d + C \rightarrow \pi^- + X) &\simeq \sigma(p + C \rightarrow \pi^- + X) + \sigma(n + C \rightarrow \pi^- + X) \\ &= \sigma(p + C \rightarrow \pi^- + X) + \sigma(p + C \rightarrow \pi^+ + X)\,. \end{aligned} \tag{3}$$

For the second equation in Eq. (3), an iso-spin conjugation is applied. The relation between proton- and α-induced reactions can be written as

$$\sigma(\alpha + C \rightarrow \pi^- + X) \simeq 2 \times \{\sigma(p + C \rightarrow \pi^- + X) + \sigma(p + C \rightarrow \pi^+ + X)\}\,. \tag{4}$$

This comparison is given in Fig. 8 as the pion momentum spectra. These agree with each other within the systematic errors.

Although negative kaons with high momenta were out of the $\bar{p}$-trigger gate because of their short TOF, the production cross sections were successfully measured at momenta of 1.0 and 1.5 GeV/c for negative kaons. Reflecting the threshold energies in elementary reactions (1.58 GeV for K^+ and 2.49 GeV for K^-), the K^+ production cross sections are about one order of magnitude larger than those of K^-. For positive kaon production the ratios between the proton- and deuteron-induced reactions are about 2 at 4.0 GeV/nucleon, but are about 3 for negative kaons. The ratio becomes larger at low-incident energies.

5. Simulation for antiproton production

Shor and coworkers simulated antiproton production using the "first-chance NN collision model" and succeeded in reproducing the cross section for proton-induced reactions [24]. The production process in this model is a single collision of nucleons with the internal motions in nuclei, and is described by integrating the elementary cross section into internal motions in the projectile and target nuclei,

$$E\frac{d^3\sigma}{dp^3} = \int d^3\boldsymbol{p}_\mathrm{p}\, f_\mathrm{p}(\boldsymbol{p}_\mathrm{p}) \int d^3\boldsymbol{p}_\mathrm{t}\, f_\mathrm{t}(\boldsymbol{p}_\mathrm{t}) \left[E\frac{d^3\sigma}{dp^3}_{NN\to\bar{p}pNN}(\sqrt{s_{NN}}) \right] . \tag{5}$$

The first integral on the right side of Eq. (5) is integrated over the internal motion of a nucleon in the projectile, where $\boldsymbol{p}_\mathrm{p}$ is the internal momentum of the nucleon in the projectile and $f(\boldsymbol{p}_\mathrm{p})$ is its distribution. The second integral is over the internal motion in the target nucleus. The cross section of the elementary process, which is written in the parentheses, is assumed to be proportional to the phase-space volume of the final four-body system, because the cross section has not been measured near to the threshold energy. The energy–momentum relation is treated as being on-shell for projectile nucleons. However, for the target nucleons it is off-shell. If a reacting nucleon in the target nucleus has an internal momentum $\boldsymbol{p}_\mathrm{t}$ (and the residual nucleus has a momentum $-\boldsymbol{p}_\mathrm{t}$), its energy ($E_\mathrm{t}$) can be described as

$$E_\mathrm{t} = M_A - \sqrt{M_{A-1}^2 + \boldsymbol{p}_\mathrm{t}^2}\,, \tag{6}$$

where M_A is the mass of the target nucleus and M_{A-1} is the mass of the residual nucleus, excluding a reacting nucleon. The internal-momentum distribution of the nucleons in the target nucleus was approximated using two Gaussian distributions: one represented the main component, and the other was an additional higher momentum component [24].

The cross sections of antiproton production in p+C reactions were first calculated with this model. The momentum spectrum and the incident-energy dependence were successfully reproduced, as shown in Fig. 9. The conversion factor from the phase-space volume to the elementary cross section was fixed by comparing the calculated values with the experimental data. Then, the deuteron-induced reactions were calculated while taking the deuteron wave-function into account (Fig. 10). The same values in a p+C calculation were used for the other parameters, such as the momentum distribution in the target nucleus and the elementary cross section (or the conversion factor). Although the proton-induced reactions were reproduced well by this model, the deuteron-induced reactions were underestimated, except for data at an incident energy of 5.0 GeV/nucleon. Two wave functions were used for the deuteron: Hulthen's function [25] and the distribution given by Haneishi and Fujita [26] (Fig. 11). Haneishi and Fujita's one (doted histogram in Fig. 10), seems to give a slightly better result than that of Hulthen (solid histogram), because a higher momentum component is included in this wave function (Fig. 11). Even with the realistic higher momentum component, the experimental data can not be reproduced. The difference between proton- and deuteron-induced re-

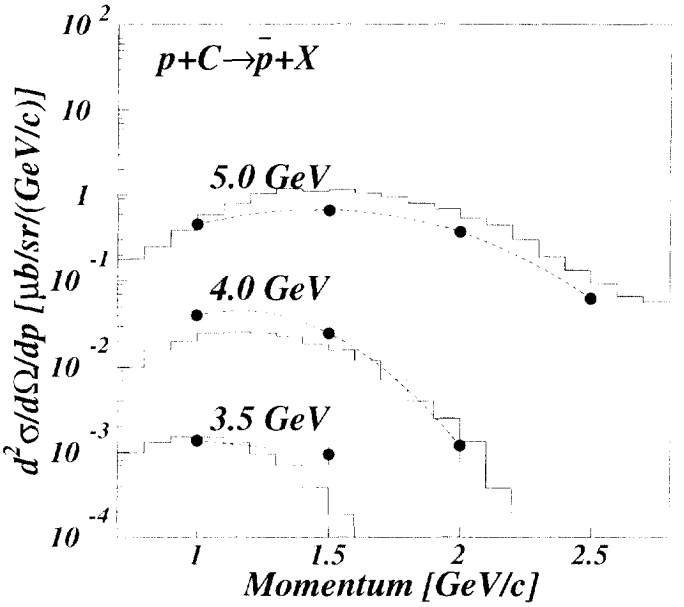

Fig. 9. Result of the "first-chance NN collision model" for p+C reactions. The histograms are the calculated cross sections. The symbol (•) indicates experimental data, which is joined with a line as a guide to the eyes.

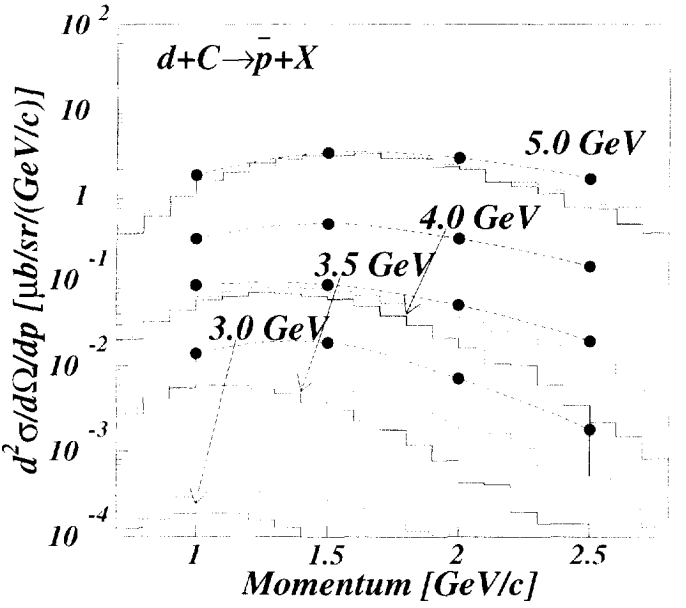

Fig. 10. Result of the "first-chance NN collision model" for d+C reactions. The solid and dotted histograms are the calculated cross sections with the deuteron wave-form of Hulthen function and the distribution of Haneishi and Fujita, respectively. The symbol (•) is the experimental data, which is joined with a line as a guide to the eyes.

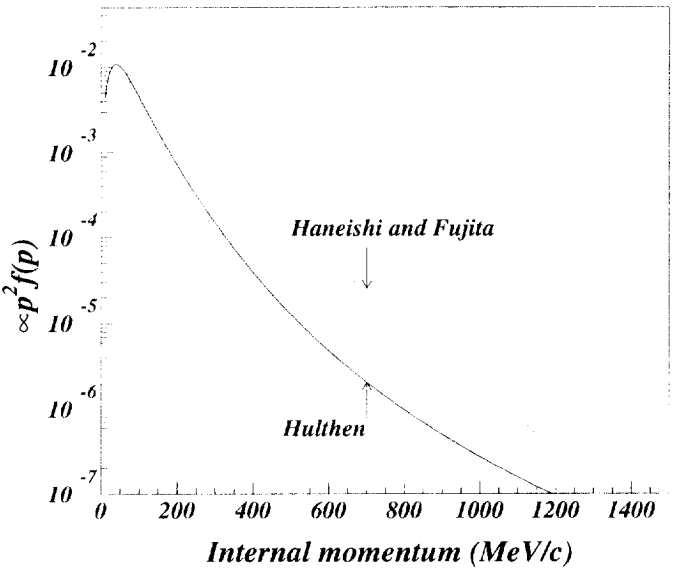

Fig. 11. Distributions of the internal momentum of a nucleon in a deuteron. The solid line is Hulthen's function [25] and the dotted line is the distribution of Haneishi and Fujita [26].

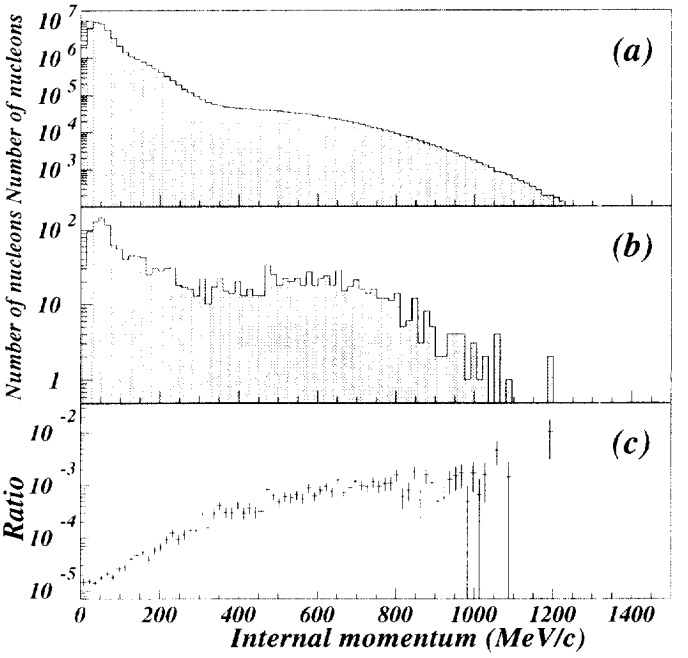

Fig. 12. Distributions which were obtained in a calculation for the d+C reaction at an incident energy of 4.0 GeV/nucleon, as a function of the internal momentum of a nucleon in the projectile; (a) the wave function (distribution of Haneishi and Fujita), (b) the momentum distribution of the nucleons which produce an antiproton and (c) the ratios of the numbers of nucleons in (b) to those in (a). These are momentum components which are parallel to the incident deuteron.

actions in this calculation is only whether internal motion in the projectile exists or not. Therefore, we carefully examined how the result is affected by the internal motion of a nucleon in a projectile deuteron for the d+C reaction at an incident energy of 4.0 GeV/nucleon. Fig. 12a shows the distribution of the internal momentum parallel to the incident deuteron; Fig. 12b is the distribution of the internal momentum for a nucleon which produces an antiproton in the first-chance NN collision model. From Fig. 12b it is clear that the high internal-momentum tail does not contribute very much to antiproton production. Fig. 12c shows the ratios of the number of nucleons in Fig. 12b to those in Fig. 12a, that is, the relative probability of the antiproton production as a function of the internal momentum of a nucleon in a projectile nucleus. Although the production probability for antiprotons becomes higher as the internal momentum increases, as we expected, the component part in the high internal-momentum tail in the deuteron wave-function is too small to account for the large antiproton-production cross section. We conclude that one can not reproduce the large cross sections of antiproton production using this model, even if the deuteron wave-function has a larger high-momentum component.

The VUU approach could successfully reproduce the large antiproton cross sections in heavy-ion collisions [13]. However, in the present status the model has hardly accounted for the large subthreshold antiproton-production cross sections in light-ion reactions because of the small nucleon number in the projectile [27].

An interaction among one nucleon in a projectile and several nucleons in a target nucleus can lead to large antiproton yields [15,28]. If the threshold energy for antiproton production is effectively reduced in nuclear matter [29], large antiproton yields are also obtained. In both cases, larger antiproton yields are produced not only in the deuteron- and α-induced reactions, but also in the proton-induced ones; therefore, to reproduce the projectile dependence of antiproton production, the internal motion in the projectile must be adopted into their arguments. W. Cassing showed that the larger antiproton-production cross sections could be caused by a strong correlation between the effect of the self-energies of baryons and the internal motion in a projectile deuteron [30]. However, the correlation was not explicitly expressed in their paper.

6. Summary

We measured the cross sections of subthreshold antiproton production systematically using proton, deuteron and α beams. The motivation of this measurement was to examine the antiproton production cross section in the case of light ions, since a large cross section had been observed in heavy-ion reactions; however unexpectedly, large cross sections were also found in the light-ion-induced reactions relative to proton-induced reactions.

The deuteron has two nucleons which are weakly bound; nevertheless, the ratio of the antiproton-production cross-section between a deuteron-induced reaction and a proton-induced one is extremely large, two orders of magnitude at an incident energy of 3.5 GeV/nucleon. The cross section in the α-induced reaction is one order larger than

that in a deuteron-induced reaction at 3.5 GeV/nucleon.

The key point for understanding the mechanism of subthreshold antiproton production in light-ion induced reactions is the large ratio between the proton-induced reaction and the deuteron-induced reaction. Experimental and theoretical research should be continued to focus on this point. That is, a comparison between deuteron- and proton-induced reactions at other production angles is needed in order to find a source of the antiproton, and an experiment with a deuteron target is required to see a simplified reaction system.

The cross sections of pion production were measured at the same time. The experimental procedure was confirmed by using the cross sections. Kaon-production cross sections were also measured in the same energy region.

Acknowledgements

We would like to express special thanks to the staff of the KEK-PS accelerator division for the successful acceleration of deuteron and α beams; in particular to Prof. M. Kihara and Prof. Y. Mori who led this light-ion program. We express sincere gratitude to members of the Beam-Channel Groups for their help during the experiment. We are grateful to the Counter-hall Groups, the Electronics and On-line Groups, the Computing Center and the Mechanical Engineering Center at KEK for their indispensable assistance. We are grateful to Prof. H. Sugawara, Prof. S. Iwata, Prof. K. Nakai, Prof. K. Nakamura and members of KEK physics department. We would like thanks to Prof. K. Niita and Dr. T. Maruyama for their theoretical support. We also would like to thank Mr. Ron Fox (MSU/NSCL) for discussion of this paper.

Appendix A. Cross section table

The differential cross sections of particle production are summarized in Tables A.1–A.15 to three significant digits. E_{in} is the incident energy per nucleon. C, Al, Cu and Pb indicate targets of carbon, aluminum, copper and lead, respectively. Statistical errors ($d\sigma = \sigma/\sqrt{N}$) are shown, where N is number of observed particles. The cross section of the pion includes electrons (positrons).

References

[1] J. Chiba et al., Nucl. Phys. A 553 (1993) 771c.
[2] J. Chiba et al., Nucl. Phys. A 583 (1995) 633c.
[3] O. Chamberlain et al., Phys. Rev. 100 (1955) 947.
[4] D. Dorfan et al., Phys. Rev. Lett. 14 (1965) 995.
[5] Yu.B. Lepikhin et al., JETP Lett. 46 (1988) 275.
[6] A.A. Baldin et al., Nucl. Phys. A 519 (1990) 407c.
[7] J. Carroll et al., Phys. Rev. Lett. 62 (1989) 1829.
[8] A. Shor et al., Phys. Rev. Lett. 63 (1989) 2192.
[9] A. Schröter et al., Nucl. Phys. A 553 (1993) 775c.

Table A.1
Differential $\overline{p}$-production cross sections in the proton-induced reactions in a unit of (μb/sr/(GeV/c))

Energy (GeV)	Target	Momentum (GeV/c)			
		1.0	1.5	2.0	2.5
5.0	C	0.451 ± 0.039	0.663 ± 0.067	0.366 ± 0.037	0.0619 ± 0.0071
	Cu	1.21 ± 0.10	1.58 ± 0.11	0.728 ± 0.062	0.108 ± 0.014
4.0	C	0.0400 ± 0.0048	0.0248 ± 0.0025	0.00118 ± 0.00045	
	Cu	0.104 ± 0.011	0.0643 ± 0.0071	0.00472 ± 0.00178	
3.5	C	0.00138 ± 0.00040	0.000941 ± 0.000243		
	Cu	0.00442 ± 0.00167			
12.0	C	53.4 ± 0.6	173 ± 1	273 ± 1	297 ± 1
	Al	100 ± 2	299 ± 6	464 ± 6	490 ± 5
	Cu	167 ± 2	486 ± 4	745 ± 4	774 ± 3
	Pb	328 ± 4	839 ± 6	1260 ± 10	1280 ± 0

Table A.2
Differential $\overline{p}$-production cross sections in the deuteron-induced reactions in a unit of (μb/sr/(GeV/c))

Energy (GeV)	Target	Momentum (GeV/c)			
		1.0	1.5	2.0	2.5
5.0	C	1.70 ± 0.03	3.12 ± 0.04	2.70 ± 0.04	1.54 ± 0.02
	Al	3.19 ± 0.07	5.53 ± 0.10	4.33 ± 0.09	2.64 ± 0.08
	Cu	4.78 ± 0.15	8.46 ± 0.17	6.88 ± 0.13	4.01 ± 0.13
	Pb	7.01 ± 0.32	11.5 ± 0.6	9.28 ± 0.42	5.26 ± 0.26
4.0	C	0.306 ± 0.014	0.457 ± 0.011	0.303 ± 0.005	0.143 ± 0.004
	Al	0.547 ± 0.028	0.863 ± 0.081	0.556 ± 0.025	0.220 ± 0.008
	Cu	0.853 ± 0.056	1.07 ± 0.06	0.745 ± 0.034	0.317 ± 0.013
	Pb	1.40 ± 0.11	1.45 ± 0.13	0.923 ± 0.090	0.411 ± 0.043
3.5	C	0.0862 ± 0.0087	0.0872 ± 0.0075	0.0505 ± 0.0039	0.0193 ± 0.0017
	Cu	0.276 ± 0.027	0.288 ± 0.019	0.143 ± 0.009	0.0533 ± 0.0064
3.0	C	0.0165 ± 0.0017	0.0176 ± 0.0012	0.00822 ± 0.00073	0.00118 ± 0.00023
	Cu	0.0320 ± 0.0073	0.0309 ± 0.0033	0.0166 ± 0.0031	0.00507 ± 0.00106
	Pb	0.0772 ± 0.0092	0.0652 ± 0.0064	0.0244 ± 0.0026	0.00685 ± 0.00123
2.5	C		0.00171 ± 0.00024	0.000204 ± 0.000091	
	Cu	0.00778 ± 0.00550	0.00295 ± 0.00048	0.00101 ± 0.00101	
	Pb		0.00498 ± 0.00100	0.00253 ± 0.00253	

[10] C. Ko and X. Ge, Phys. Lett. B 205 (1988) 195.
[11] C. Ko and L. Xia, Phys. Rev. C 40 (1989) R1118.
[12] P. Koch and C. Dover, Phys. Rev. C 40 (1989) 145.
[13] G. Batko et al., Phys. Lett. B 256 (1991) 331.
[14] S. Huang et al., Nucl. Phys. A 547 (1992) 653.
[15] P. Danielewicz, Phys. Rev. C 42 (1990) 1564.
[16] M. Ieiri et al., *in* Proc. 9th Symposium on accelerator Science and Technology, 1993, p. 477.
[17] M. Numajiri, private communication.
[18] Y. Sugaya et al., Nucl. Instr. and Meth. A 368 (1996) 635.
[19] K.H. Tanaka et al., *in* Proc. Workshop in Advanced Beam Instrumentation, KEK Proc. 91-2 (1991) A145.
[20] Y. Takada, private communication.
[21] H. Aihara et al., Nucl. Phys. A 360 (1981) 291.

Table A.3
Differential $\bar{p}$-production cross sections in the α-induced reactions in a unit of (μb/sr/(GeV/c))

Energy (GeV)	Target	Momentum (GeV/c)			
		1.0	1.5	2.0	2.5
5.0	C	6.17 ± 0.19	11.9 ± 0.3	12.4 ± 0.3	9.04 ± 0.23
	Al	10.8 ± 0.5			
	Cu	19.2 ± 0.8	32.7 ± 1.4	30.9 ± 1.2	23.3 ± 1.1
4.0	C	1.89 ± 0.12	3.10 ± 0.19	2.64 ± 0.15	1.48 ± 0.08
	Al	3.47 ± 0.34	5.42 ± 0.45		
	Cu	5.34 ± 0.35	8.59 ± 0.43	6.77 ± 0.33	4.46 ± 0.24
3.5	C	0.800 ± 0.059	1.11 ± 0.07	0.703 ± 0.070	0.469 ± 0.032
	Cu	1.97 ± 0.17	3.16 ± 0.22	2.34 ± 0.15	1.09 ± 0.08
3.0	C	0.241 ± 0.034	0.223 ± 0.029	0.123 ± 0.016	0.0825 ± 0.0097
	Cu	0.603 ± 0.107	0.641 ± 0.103	0.421 ± 0.080	0.181 ± 0.027
2.5	C		0.0301 ± 0.0056		
	Cu	0.0763 ± 0.0197	0.101 ± 0.020	0.0339 ± 0.0102	
2.0	Cu		0.00332 ± 0.00235		

Table A.4
Differential K^+-production cross sections in the proton-induced reactions in a unit of (mb/sr/(GeV/c))

Energy (GeV)	Target	Momentum (GeV/c)			
		1.0	1.5	2.0	2.5
5.0	C	5.80 ± 0.83	4.94 ± 0.69	4.02 ± 0.48	
	Cu	25.6 ± 3.1	14.5 ± 2.1	10.7 ± 2.1	
4.0	C		3.74 ± 0.55	1.78 ± 0.29	
	Cu	13.8 ± 1.8	10.4 ± 1.4	4.59 ± 0.70	
12.0	C	16.0 ± 0.8	19.9 ± 0.6	18.7 ± 0.4	17.3 ± 0.3
	Al	30.5 ± 2.6	33.8 ± 1.2	31.8 ± 1.4	30.4 ± 0.8
	Cu	58.6 ± 3.1	71.0 ± 1.8	64.5 ± 1.2	53.7 ± 1.2
	Pb	210 ± 17	180 ± 7	160 ± 5	

[22] Review of Particle Properties, Phys. Rev. D 50 (1994).
[23] S.H. Kahana et al., Phys. Rev. C 47 (1993) 47.
[24] A. Shor et al., Nucl. Phys. A 514 (1990) 717.
[25] L. Hulthen and M. Sugawara, The Two-Nucleon Problem, Encyclopedia of Physics, Vol.XXXIX, ed. S. Flügge (Springer-Verlag, Berlin, 1957) p. 1.
[26] Y. Haneishi and T. Fujita, Phys. Rev. C 33 (1986) 260.
[27] K. Niita and T. Maruyama, private communication.
[28] E. Hernández et al., Z. Phys. A 351 (1995) 99.
[29] S. Teis et al., Phys. Rev. C 50 (1994) 388.
[30] W. Cassing et al., Z. Phys. A 348 (1994) 247.

Table A.5
Differential K^+-production cross sections in the deuteron-induced reactions in a unit of (mb/sr/(GeV/c))

Energy (GeV)	Target	Momentum (GeV/c)			
		1.0	1.5	2.0	2.5
5.0	C	10.6 ± 1.2	11.3 ± 0.5	8.53 ± 0.54	
	Al	21.3 ± 2.8	19.9 ± 2.4	13.3 ± 1.4	
	Cu	35.5 ± 5.2	26.9 ± 5.5	23.4 ± 2.9	
	Pb	77.1 ± 9.9	65.8 ± 4.4	43.2 ± 2.4	
4.0	C	7.35 ± 0.77	5.89 ± 0.55	4.09 ± 0.27	
	Al	10.1 ± 1.8	10.4 ± 1.9		
	Cu	24.4 ± 3.6	18.3 ± 2.9	9.56 ± 1.19	
	Pb	54.7 ± 7.4	24.8 ± 4.1	17.3 ± 1.4	
3.5	C	4.89 ± 0.80	3.79 ± 0.66	2.31 ± 0.53	
	Cu	15.3 ± 2.2	9.61 ± 1.65	4.68 ± 1.33	
3.0	C	2.88 ± 0.49	1.75 ± 0.18		
	Cu		3.27 ± 0.91		
	Pb	12.9 ± 2.6	7.20 ± 0.95	2.52 ± 0.42	
2.5	C	1.81 ± 0.47	0.517 ± 0.138		
	Cu	4.26 ± 1.14	1.38 ± 0.35		
	Pb	8.00 ± 2.14	2.76 ± 0.65	0.628 ± 0.237	

Table A.6
Differential K^+-production cross sections in the α-induced reactions in a unit of (mb/sr/(GeV/c))

Energy (GeV)	Target	Momentum (GeV/c)			
		1.0	1.5	2.0	2.5
5.0	C	24.5 ± 2.3	20.9 ± 1.4	17.2 ± 1.0	11.3 ± 0.8
	Al	43.8 ± 4.0	32.7 ± 2.3	26.1 ± 1.4	20.3 ± 0.9
	Cu		72.1 ± 4.1	48.2 ± 2.3	34.1 ± 1.5
4.0	C	15.8 ± 1.6	13.9 ± 1.2	9.25 ± 0.65	4.89 ± 0.45
	Al	27.7 ± 3.3	21.6 ± 2.1	14.7 ± 1.2	7.93 ± 0.78
	Cu	53.5 ± 5.4	42.4 ± 3.4	22.4 ± 1.7	12.7 ± 1.0
3.5	C	11.8 ± 1.5	9.20 ± 0.92	6.26 ± 0.56	2.86 ± 0.35
	Cu	31.9 ± 4.3	27.1 ± 2.7	16.0 ± 1.5	7.15 ± 0.82
3.0	C	6.82 ± 1.14	5.32 ± 0.66	1.97 ± 0.32	1.07 ± 0.21
	Cu	22.7 ± 3.6	12.2 ± 1.7	7.52 ± 0.96	2.28 ± 0.47
2.5	C	5.41 ± 1.02	3.22 ± 0.45	0.954 ± 0.203	0.387 ± 0.129
	Cu	12.8 ± 2.7	5.84 ± 0.99	2.66 ± 0.53	0.855 ± 0.270
2.0	Cu	2.51 ± 1.78	4.52 ± 1.51		

Table A.7
Differential K^--production cross sections in the proton-induced reactions in a unit of (mb/sr/(GeV/c))

Energy (GeV)	Target	Momentum (GeV/c)			
		1.0	1.5	2.0	2.5
5.0	Cu		1.03 ± 0.04		
4.0	C		0.118 ± 0.001		
	Cu		0.290 ± 0.003		
3.5	C		0.0209 ± 0.0005		
12.0	C	5.49 ± 0.06	6.61 ± 0.02		
	Al	11.2 ± 0.2	11.2 ± 0.1		
	Cu	21.1 ± 0.2	22.2 ± 0.1		
	Pb	44.2 ± 0.7	45.7 ± 0.3		

Table A.8
Differential K^--production cross sections in the deuteron-induced reactions in a unit of (mb/sr/(GeV/c))

Energy (GeV)	Target	Momentum (GeV/c)			
		1.0	1.5	2.0	2.5
5.0	C		1.20 ± 0.01		
	Al		2.07 ± 0.02		
	Cu		2.87 ± 0.03		
	Pb		5.16 ± 0.04		
4.0	C		0.398 ± 0.002		
	Al	1.12 ± 0.04	0.581 ± 0.014		
	Cu	1.86 ± 0.06	0.861 ± 0.011		
	Pb		1.57 ± 0.01		
3.5	C		0.141 ± 0.004		
	Cu		0.373 ± 0.011		
3.0	C		0.0395 ± 0.0003		
	Cu		0.0638 ± 0.0036		
	Pb		0.156 ± 0.001		
2.5	C	0.0313 ± 0.0015	0.00674 ± 0.00005		
	Cu	0.0773 ± 0.0037	0.0165 ± 0.0001		
	Pb	0.127 ± 0.007	0.0242 ± 0.0002		

Table A.9
Differential K^--production cross sections in the α-induced reactions in a unit of (mb/sr/(GeV/c))

Energy (GeV)	Target	Momentum (GeV/c)			
		1.0	1.5	2.0	2.5
5.0	C	3.55 ± 0.03	2.51 ± 0.02		
	Al	6.27 ± 0.07			
	Cu	11.9 ± 0.1	7.44 ± 0.07		
4.0	C	1.93 ± 0.03	1.14 ± 0.01		
	Al	3.35 ± 0.07	1.86 ± 0.03		
	Cu	6.29 ± 0.08	3.08 ± 0.03		
3.5	C	1.25 ± 0.02	0.573 ± 0.006		
	Cu	3.92 ± 0.05	1.64 ± 0.02		
3.0	C	0.490 ± 0.010	0.195 ± 0.003		
	Cu	1.46 ± 0.04	0.528 ± 0.011		
2.5	C		0.0556 ± 0.0009		
	Cu	0.585 ± 0.012	0.152 ± 0.003		
2.0	Cu		0.0183 ± 0.0006		

Table A.10
Differential π^+-production cross sections in the proton-induced reactions in a unit of (mb/sr/(GeV/c))

Energy (GeV)	Target	Momentum (GeV/c)			
		1.0	1.5	2.0	2.5
5.0	C	186 ± 1	211 ± 1	133 ± 1	67.2 ± 0.5
	Cu	495 ± 2	485 ± 2	298 ± 2	138 ± 1
4.0	C	172 ± 3	178 ± 1	68.4 ± 0.4	29.9 ± 0.3
	Cu	412 ± 2	390 ± 2	144 ± 1	58.6 ± 1.1
3.5	C	116 ± 2	90.8 ± 1.5	30.1 ± 0.5	9.97 ± 0.23
	Cu	271 ± 5	190 ± 3	46.6 ± 0.9	18.4 ± 0.4
12.0	C	327 ± 1	350 ± 1	338 ± 1	282 ± 1
	Al	616 ± 2	588 ± 2	535 ± 3	427 ± 2
	Cu	1240 ± 1	1080 ± 1	940 ± 2	761 ± 2
	Pb	2510 ± 10	2010 ± 10	1740 ± 10	1420 ± 10

Table A.11
Differential π^+-production cross sections in the deuteron-induced reactions in a unit of (mb/sr/(GeV/c))

Energy (GeV)	Target	Momentum (GeV/c)			
		1.0	1.5	2.0	2.5
5.0	C	289 ± 1	283 ± 1	180 ± 1	89.4 ± 0.4
	Al	508 ± 2	451 ± 2	278 ± 2	134 ± 1
	Cu	832 ± 4	716 ± 5	430 ± 3	147 ± 2
	Pb	1300 ± 10	1000 ± 10	614 ± 4	297 ± 2
4.0	C	224 ± 1	197 ± 1	84.1 ± 0.4	36.4 ± 0.3
	Al	334 ± 2	267 ± 2	113 ± 1	46.3 ± 0.7
	Cu	532 ± 3	411 ± 3	170 ± 2	69.4 ± 1.1
	Pb	931 ± 5	689 ± 7	284 ± 2	122 ± 1
3.5	C	215 ± 1	151 ± 1	53.6 ± 0.5	18.5 ± 0.3
	Cu	477 ± 2	304 ± 2	102 ± 1	
3.0	C	128 ± 1	62.4 ± 0.3	18.9 ± 0.2	4.22 ± 0.10
	Cu	345 ± 5	152 ± 1	42.3 ± 0.6	7.83 ± 0.58
	Pb	443 ± 3	186 ± 1	53.8 ± 0.8	12.9 ± 0.4
2.5	C	122 ± 1	31.5 ± 0.3	6.12 ± 0.15	1.07 ± 0.07
	Cu	252 ± 1	61.1 ± 0.7	12.2 ± 0.3	1.43 ± 0.11
	Pb	387 ± 2	90.9 ± 1.1	18.2 ± 0.5	2.17 ± 0.16

Table A.12
Differential π^+-production cross sections in the α-induced reactions in a unit of (mb/sr/(GeV/c))

Energy (GeV)	Target	Momentum (GeV/c)			
		1.0	1.5	2.0	2.5
5.0	C	587 ± 2	540 ± 2	340 ± 2	166 ± 1
	Al	990 ± 3	826 ± 4	509 ± 3	253 ± 2
	Cu		1300 ± 10	787 ± 4	385 ± 3
4.0	C	498 ± 1	412 ± 2	189 ± 1	77.1 ± 0.9
	Al	804 ± 3	607 ± 3	278 ± 2	112 ± 1
	Cu	1310 ± 1	930 ± 5	416 ± 3	167 ± 2
3.5	C	450 ± 2	315 ± 2	117 ± 1	43.8 ± 0.7
	Cu	1090 ± 1	690 ± 4	259 ± 2	91.2 ± 1.5
3.0	C	351 ± 1	182 ± 1	53.8 ± 0.7	16.7 ± 0.4
	Cu	817 ± 4	382 ± 3	112 ± 2	33.6 ± 0.9
2.5	C	318 ± 1	105 ± 1	24.1 ± 0.4	6.02 ± 0.26
	Cu	691 ± 3	218 ± 2	49.2 ± 1.0	11.9 ± 0.5
2.0	Cu	373 ± 4	63.9 ± 1.8	11.5 ± 0.9	1.65 ± 0.40

Table A.13
Differential π^--production cross sections in the proton-induced reactions in a unit of (mb/sr/(GeV/c))

Energy (GeV)	Target	Momentum (GeV/c)			
		1.0	1.5	2.0	2.5
5.0	C	95.6 ± 0.6	74.3 ± 0.8	42.4 ± 0.4	23.5 ± 0.1
	Cu	280 ± 2	188 ± 1	102 ± 1	51.8 ± 0.3
4.0	C	73.7 ± 0.2	49.3 ± 0.1	22.4 ± 0.1	
	Cu	198 ± 1	121 ± 1	50.0 ± 0.2	
3.5	C	39.2 ± 0.1	22.4 ± 0.1		
	Cu	77.2 ± 0.2			
12.0	C	301 ± 2	283 ± 1	259 ± 1	197 ± 1
	Al	663 ± 6	559 ± 8	458 ± 7	333 ± 4
	Cu	1290 ± 10	985 ± 6	781 ± 4	579 ± 3
	Pb	2490 ± 10	1770 ± 10	1380 ± 10	1020 ± 1

Table A.14
Differential π^--production cross sections in the deuteron-induced reactions in a unit of (mb/sr/(GeV/c))

Energy (GeV)	Target	Momentum (GeV/c)			
		1.0	1.5	2.0	2.5
5.0	C	265 ± 1	275 ± 1	183 ± 1	89.8 ± 0.2
	Al	491 ± 1	444 ± 1	275 ± 1	135 ± 1
	Cu	798 ± 2	690 ± 2	419 ± 1	204 ± 1
	Pb	1250 ± 1	1000 ± 10	611 ± 4	296 ± 2
4.0	C	201 ± 1	200 ± 1	84.9 ± 0.1	37.0 ± 0.1
	Al	337 ± 1	323 ± 2	135 ± 1	52.7 ± 0.1
	Cu	520 ± 1	459 ± 1	193 ± 1	75.4 ± 0.2
	Pb	871 ± 3	710 ± 3	263 ± 2	111 ± 1
3.5	C	189 ± 1	145 ± 1	50.3 ± 0.1	19.1 ± 0.1
	Cu	482 ± 1	325 ± 1	105 ± 1	37.7 ± 0.2
3.0	C	129 ± 1	63.3 ± 0.1	18.5 ± 0.1	4.95 ± 0.01
	Cu	309 ± 1	140 ± 1	41.0 ± 0.2	10.1 ± 0.1
	Pb	569 ± 1	244 ± 1	64.9 ± 0.1	14.4 ± 0.1
2.5	C	113 ± 1	30.0 ± 0.1	6.44 ± 0.02	
	Cu	249 ± 1	58.9 ± 0.1	13.9 ± 0.1	
	Pb	405 ± 2	86.2 ± 0.1	15.6 ± 0.2	

Table A.15
Differential π^--production cross sections in the α-induced reactions in a unit of (mb/sr/(GeV/c))

Energy (GeV)	Target	Momentum (GeV/c)			
		1.0	1.5	2.0	2.5
5.0	C	592 ± 2	554 ± 2	342 ± 2	163 ± 1
	Al	1000 ± 1			
	Cu	1730 ± 10	1350 ± 10	800 ± 6	377 ± 5
4.0	C	527 ± 2	428 ± 2	193 ± 1	76.0 ± 0.6
	Al	833 ± 6	625 ± 5		
	Cu	1460 ± 10	1000 ± 10	439 ± 3	172 ± 2
3.5	C	486 ± 2	316 ± 1	114 ± 1	41.1 ± 0.3
	Cu	1280 ± 1	748 ± 4	270 ± 2	93.7 ± 0.8
3.0	C	336 ± 1	177 ± 1	52.6 ± 0.4	16.3 ± 0.1
	Cu	817 ± 4	370 ± 3	109 ± 1	34.3 ± 0.4
2.5	C		98.6 ± 0.4		
	Cu	703 ± 2	208 ± 1	48.9 ± 0.4	
2.0	Cu		62.2 ± 0.4		